

## Spin dynamics of stripes

Frank Krüger and Stefan Scheidl

*Institut für Theoretische Physik, Universität zu Köln, Zùlpicher Strasse 77, D-50937 Köln, Germany*

(Received 25 November 2002; published 4 April 2003)

The spin dynamics of stripes in high-temperature superconductors and related compounds is studied in the framework of a spin-wave theory for a simple spin-only model. The magnon dispersion relation and the magnetic structure factor are calculated for diagonal and vertical stripes. Acoustical as well as optical bands are included in the analysis. The incommensuration and the  $\pi$  resonance appear as complementary features of the band structure at different energy scales. The dependence of spin-wave velocities and resonance frequencies on the stripe spacing and coupling is calculated. At low doping, the resonance frequency is found to scale roughly inversely proportional to the stripe spacing. The favorable comparison of the results with experimental data suggests that the spin-only model provides a suitable and simple basis for calculating and understanding the spin dynamics of stripes.

DOI: 10.1103/PhysRevB.67.134512

PACS number(s): 75.10.Jm, 74.72.-h, 75.30.Fv, 76.50.+g

### I. INTRODUCTION

The evidence for the formation of stripes in high-temperature superconductors (HTSC's) and related materials increases continuously. After the theoretical prediction<sup>1-3</sup> of stripes as a combined charge and spin-density wave phenomenon, years passed until a broad interest was triggered by experiments on insulating  $\text{La}_{2-x}\text{Sr}_x\text{NiO}_{4+\delta}$  (LSNO) and superconducting  $\text{La}_{2-x}\text{Sr}_x\text{CuO}_4$  (LSCO).<sup>4,5</sup> More recent experimental evidence<sup>6-9</sup> for stripes in the paradigmatic HTSC's  $\text{YBaCuO}_{6+\delta}$  (YBCO) and  $\text{Bi}_2\text{Sr}_2\text{CaCu}_2\text{O}_{8+\delta}$  (BSCCO) strengthens the expectation that stripe formation in doped layered perovskites is quite generic.

In spite of the striking evidence for stripes in HTSC's, the causal connection between stripe formation and superconductivity still is a mystery. It is puzzling that both phenomena coexist and that, nevertheless, stripes tend to suppress superconductivity.<sup>10,11</sup> For this interplay, spin order is more relevant than charge order. In particular, the strength of spin fluctuations appears to play a central role. Static spin order seems to be much less compatible with superconductivity than dynamic spin order.

At present, one important open question is to what extent the stripe picture can account for spin fluctuations not only at low energies, where collective magnetic excitations are observed at satellite positions in the vicinity of the antiferromagnetic wave vector, but also over a wider energy range, including the resonance phenomenon at the antiferromagnetic wave vector (see Refs. 12 and 13, and references therein). The specific form of the dynamic magnetic response—including “incommensuration” (the separation between the satellite position and the antiferromagnetic wave vector) and  $\pi$  resonance—gave rise to doubts that it could be consistent with the stripe picture.<sup>14</sup> On the other hand, there are proposals<sup>15</sup> that both features may be rooted in a stripe-like spin-density wave.

In this paper, we complement the spin-wave analysis by Batista *et al.*<sup>15</sup> There, the emphasis was put on generic features of striped systems for an arbitrary ratio between the spin spacing  $a$  and the stripe spacing  $d$ . For general ratios the structure of the magnetic excitation spectrum can be quite

intricate due to the coupling of a large number of modes with different wave vectors. However, in many cases of interest, this ratio  $p:=d/a$  is very close to an integer value. For stripes—like for any density waves—one actually expects that integer values  $p$  are energetically very stable due to a lock-in of the superstructure into the atomic structure. This pinning mechanism is considered as the origin of the so-called “1/8 conundrum” in the cuprates,<sup>5</sup> i.e., the stability of  $p=4$  over a considerable doping range. Detailed measurements of the spin-excitation spectrum are available close to integer  $p$ :  $p=3$  in LSNO,<sup>16</sup>  $p=4$  in LSCO,<sup>17</sup> and  $p=4$  (Ref. 18) and  $p=5$  (Ref. 14) in YBCO.

In order to test whether these experiments can be consistent with the spin-wave excitation spectrum of a stripe model in the simplest and most transparent case, we therefore examine integer  $p$ . In this case a stripe state can be conveniently modeled as a periodic structure on the square lattice of possible electron/hole positions. The magnetic excitations are studied in the framework of a spin-only model that does not fully account for electronic correlations. In particular, a possible spin gap at very low energies due to the formation of Cooper pairs is not incorporated. Nevertheless, one can expect an adequate description of spin fluctuations well above the gap energy. This energy range also includes the  $\pi$  resonance.

Particular attention is paid to the spin-wave band structure in the vicinity of the antiferromagnetic wave vector. While the zero-frequency incommensuration<sup>19</sup> is fixed by the geometry of the model, we calculate the spin-wave velocities and the  $\pi$  resonance as dynamic features. We evaluate the dependence of these quantities on the stripe period (respectively, the doping level) and the exchange coupling across the stripes. By a quantitative comparison, we determine the value of the exchange coupling across the stripes as the only *a priori* unknown model parameter. In particular, the dependence of the  $\pi$  resonance on doping is found to be consistent with experiments.

Our course starts in Sec. II with the introduction of the spin-only model that constitutes the basis of our study. The linear spin-wave theory is outlined in Sec. III. In Sec. IV, we present numerical results for the magnon dispersion relation,

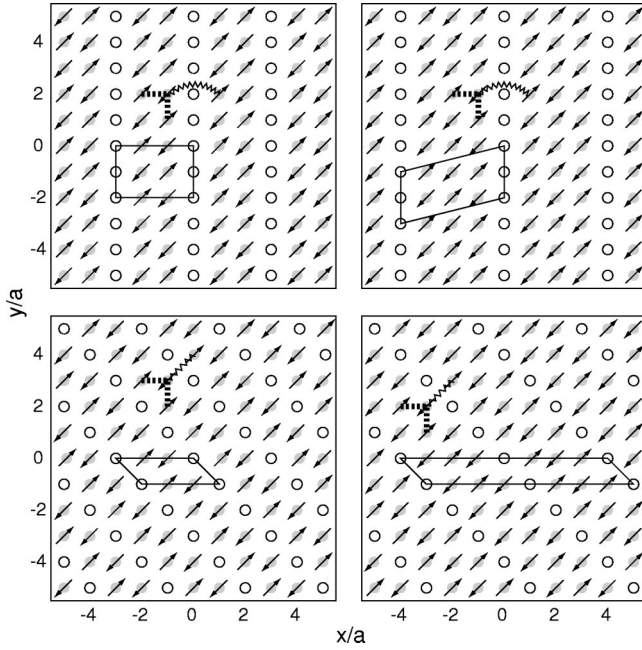


FIG. 1. Illustration of vertical and diagonal stripe patterns with spacings  $p=3$  and  $p=4$ . The hole positions are indicated by open circles and the electron positions by gray ones. The arrows correspond to the spin orientations in the classical ground state. Parallelograms outline magnetic unit cells spanned by  $\mathbf{A}^{(1)}$  and  $\mathbf{A}^{(2)}$ . In our model, we assume antiferromagnetic exchange couplings of strength  $J$  within the domains (dashed lines) and  $\lambda J$  across stripes (zigzag lines).

spin-wave velocities,  $\pi$  resonance, and the structure factor. In Sec. V, the results of our theory are discussed and compared to experimental data.

## II. MODEL

In the cuprates as well as in the nickelates, the metallic spins are located on square lattices in weakly coupled layers. Since the interlayer coupling generally is much smaller than the intralayer coupling, we focus on a single layer. For simplicity, the holes induced by doping are assumed to form site-centered rivers that act like antiphase boundaries for the antiferromagnetic domains.<sup>5</sup> The rivers are assumed to be only one lattice spacing wide (cf. Fig. 1).

Since stripes are vertical in cuprates for doping concentrations where superconductivity occurs and diagonal in nickelates, we study both orientations with arbitrary integer stripe spacing  $p$ . Furthermore, since charge order seems to be static up to high temperatures, in YBCO up to 300 K,<sup>18</sup> holes can be considered as immobile at low temperatures. Our analysis is restricted to  $T=0$ .

We are interested in collective excitations around a ground state, which—for classical spins—could be represented by  $\mathbf{S}(\mathbf{r})=S\{0,0,\sigma(\mathbf{r})\}$  with  $\sigma=\pm 1$  on the electron positions and  $\sigma=0$  on the hole positions (as illustrated in Fig. 1). Denoting by  $\mathbf{A}^{(1)}$  and  $\mathbf{A}^{(2)}$  the primitive basis vectors of the magnetic unit cell and by  $\mathbf{A}=m_1\mathbf{A}^{(1)}+m_2\mathbf{A}^{(2)}$  an arbitrary magnetic lattice vector, the classical spin variables obey the translational symmetry  $\sigma(\mathbf{r})=\sigma(\mathbf{r}+\mathbf{A})$ . By placing

the origin at a hole position we obtain the additional reflection symmetry  $\sigma(\mathbf{r})=-\sigma(-\mathbf{r})$ .

For a paradigmatic and minimalistic description of magnetic quantum fluctuations, we use a spin-only model with pair exchange. More complicated exchange processes such as cyclic exchange<sup>20,21</sup> may be important for quantitative purposes but are ignored here for simplicity. We use a generalized Heisenberg model on the two-dimensional square lattice<sup>22</sup>

$$\mathcal{H}=\frac{1}{2}\sum'_{\mathbf{r},\mathbf{r}'}J(\mathbf{r},\mathbf{r}')\mathbf{S}(\mathbf{r})\mathbf{S}(\mathbf{r}'), \quad (1)$$

where the primed sums run over all spin positions with  $\sigma\neq 0$ . The exchange couplings obey the symmetry relations

$$J(\mathbf{r},\mathbf{r}')=J(\mathbf{r}',\mathbf{r}), \quad (2a)$$

$$J(\mathbf{r},\mathbf{r}')=J(\mathbf{r}+\mathbf{A},\mathbf{r}'+\mathbf{A}), \quad (2b)$$

$$J(\mathbf{r},\mathbf{r}')=J(-\mathbf{r},-\mathbf{r}'). \quad (2c)$$

In fact, the exchange couplings may have a higher symmetry corresponding to the hole lattice, which, however, will not be needed explicitly in the further analysis. To implement that the hole strings act as antiphase boundaries between antiferromagnetic domains, we assume that  $J(\mathbf{r},\mathbf{r}')=J>0$  for nearest neighbors  $\mathbf{r}, \mathbf{r}'$  within the domains and  $J(\mathbf{r},\mathbf{r}')=\lambda J>0$  for nearest neighbors across a string.

While it is natural to assume that  $J$  should be comparable to the exchange coupling in the undoped material, the coupling  $\lambda J$  may deviate significantly. To keep the number of parameters small, we ignore that the exchange coupling even within an antiferromagnetic domain should depend on the position of the pair relative to the hole strings.

## III. SPIN-WAVE THEORY

We address the spin dynamics in the framework of linear spin-wave theory (for a review in the context of cuprates, see, e.g., Ref. 23). In the following analytic part we keep the general form of the model and specialize to specific stripe configurations later in Sec. IV when we numerically evaluate the results of this section. From now on all lengths are expressed in units of the square-lattice spacing  $a$ .

### A. Holstein-Primakoff representation

In the first step, we flip all spins on one sublattice by

$$S^x(\mathbf{r})=\sigma^2(\mathbf{r})\tilde{S}^x(\mathbf{r}), \quad (3a)$$

$$S^y(\mathbf{r})=\sigma(\mathbf{r})\tilde{S}^y(\mathbf{r}), \quad (3b)$$

$$S^z(\mathbf{r})=\sigma(\mathbf{r})\tilde{S}^z(\mathbf{r}). \quad (3c)$$

This transformation preserves the spin commutator relations. Thereby, we allow  $\tilde{\mathbf{S}}$  to have spin  $S$  also at the hole sites. Although this introduces certain modes of zero energy, as we

will discuss below, it is advantageous to use a  $\tilde{\mathbf{S}}$  with a *homogeneous* ferromagnetic ground state.

The corresponding transformed Hamiltonian reads

$$\mathcal{H} = \frac{1}{2} \sum_{\mathbf{r}, \mathbf{r}'} \tilde{J}(\mathbf{r}, \mathbf{r}') [\tilde{S}^z(\mathbf{r}) \tilde{S}^z(\mathbf{r}') + \tilde{S}^y(\mathbf{r}) \tilde{S}^y(\mathbf{r}') + \sigma(\mathbf{r}) \sigma(\mathbf{r}') \tilde{S}^x(\mathbf{r}) \tilde{S}^x(\mathbf{r}')], \quad (4)$$

where we have defined the new couplings  $\tilde{J}(\mathbf{r}, \mathbf{r}') := J(\mathbf{r}, \mathbf{r}') \sigma(\mathbf{r}) \sigma(\mathbf{r}')$  which obey the same symmetry relations (2) as  $J$ .

In the next step, we represent the spin operators by the usual Holstein-Primakoff (HP) bosons via

$$\tilde{S}^+ = \sqrt{2S - \hat{n}} b, \quad (5a)$$

$$\tilde{S}^- = b^\dagger \sqrt{2S - \hat{n}}, \quad (5b)$$

$$\tilde{S}^z = -\hat{n} + S, \quad (5c)$$

with  $\tilde{S}^\pm = \tilde{S}^x \pm i\tilde{S}^y$ . The eigenstates of the number operator  $\hat{n} = b^\dagger b$  are restricted to  $n \leq 2S$  and the HP operators fulfill the canonical commutator relations  $[b, b^\dagger] = 1$ . The linearized spin-wave Hamiltonian  $\mathcal{H}_{\text{sw}}$  is given by the terms quadratic in the bosonic operators,

$$\mathcal{H}_{\text{sw}} = \frac{S}{2} \sum_{\mathbf{r}, \mathbf{r}'} \{f(\mathbf{r}, \mathbf{r}') [b^\dagger(\mathbf{r}) b(\mathbf{r}') + b(\mathbf{r}) b^\dagger(\mathbf{r}')] + g(\mathbf{r}, \mathbf{r}') [b(\mathbf{r}) b(\mathbf{r}') + b^\dagger(\mathbf{r}) b^\dagger(\mathbf{r}')]\}, \quad (6a)$$

$$f(\mathbf{r}, \mathbf{r}') = \frac{1}{2} \tilde{J}(\mathbf{r}, \mathbf{r}') [\sigma(\mathbf{r}) \sigma(\mathbf{r}') + 1] - \delta_{\mathbf{r}, \mathbf{r}'} \sum_{\mathbf{r}''} \tilde{J}(\mathbf{r}, \mathbf{r}''), \quad (6b)$$

$$g(\mathbf{r}, \mathbf{r}') = \frac{1}{2} \tilde{J}(\mathbf{r}, \mathbf{r}') [\sigma(\mathbf{r}) \sigma(\mathbf{r}') - 1]. \quad (6c)$$

Obviously the functions  $f$  and  $g$  again satisfy the symmetry relations (2).

For further manipulations it is useful to decompose a vector  $\mathbf{r} = \mathbf{A} + \mathbf{a}$  on the square lattice into a vector  $\mathbf{A} = m_1 \mathbf{A}^{(1)} + m_2 \mathbf{A}^{(2)}$  on the magnetic lattice and a decoration vector  $\mathbf{a}$ . The number of vectors  $\mathbf{a}$  is denoted by  $N$  (the area of the magnetic unit cell). In momentum space, the reciprocal magnetic basis  $\mathbf{Q}^{(i)}$  defines the corresponding magnetic Brillouin zone (BZ). Wave vectors  $\mathbf{k}$  can be uniquely decomposed into  $\mathbf{k} = \mathbf{Q} + \mathbf{q}$  with  $\mathbf{q} \in \text{BZ}$  and  $\mathbf{Q} = m_1 \mathbf{Q}^{(1)} + m_2 \mathbf{Q}^{(2)}$ . Within the Brillouin zone of the square lattice there are  $N$  vectors  $\mathbf{Q}$  which we denote by  $\mathbf{Q}_\nu$ .

We Fourier transform the bosonic operators via  $b(\mathbf{r}) = \int_{\mathbf{k}} \exp(i\mathbf{k} \cdot \mathbf{r}) b(\mathbf{k})$ , where  $\int_{\mathbf{k}} = (2\pi)^{-2} \int d^2k$  and the  $\mathbf{k}$  integrals run over the Brillouin zone of the square lattice with an area  $(2\pi)^2$ . Using these decompositions and the Poisson sum formula

$$\sum_{\mathbf{A}} e^{i\mathbf{k} \cdot \mathbf{A}} = \frac{1}{N} \sum_{\mathbf{Q}} \delta(\mathbf{k} + \mathbf{Q}), \quad (7)$$

we rewrite the spin-wave Hamiltonian as

$$\mathcal{H}_{\text{sw}} = \frac{1}{2} \int_{\mathbf{q}, \nu, \nu'} F_{\nu, \nu'}(\mathbf{q}) [b_{\mathbf{q} + \mathbf{Q}_\nu}^\dagger b_{\mathbf{q} + \mathbf{Q}_{\nu'}} + b_{-\mathbf{q} - \mathbf{Q}_\nu} b_{-\mathbf{q} - \mathbf{Q}_{\nu'}}^\dagger] + \frac{1}{2} \int_{\mathbf{q}, \nu, \nu'} G_{\nu, \nu'}(\mathbf{q}) [b_{\mathbf{q} + \mathbf{Q}_\nu}^\dagger b_{-\mathbf{q} - \mathbf{Q}_{\nu'}}^\dagger + b_{-\mathbf{q} - \mathbf{Q}_\nu} b_{\mathbf{q} + \mathbf{Q}_{\nu'}}], \quad (8)$$

where

$$F_{\nu, \nu'}(\mathbf{q}) = \frac{S}{N} \sum_{\mathbf{A}} \sum_{\mathbf{a}, \mathbf{a}'} f(\mathbf{a} + \mathbf{A}, \mathbf{a}') \cos[\mathbf{q} \cdot \mathbf{A} + \mathbf{q}(\mathbf{a} - \mathbf{a}') + \mathbf{Q}_\nu \cdot \mathbf{a} - \mathbf{Q}_{\nu'} \cdot \mathbf{a}'] \quad (9)$$

is essentially the Fourier transform of  $f$ ,

$$\frac{S}{N} f(\mathbf{Q}_\nu + \mathbf{q}, \mathbf{Q}_{\nu'} + \mathbf{q}') = \delta(\mathbf{q} + \mathbf{q}') F_{\nu, \nu'}(\mathbf{q}). \quad (10)$$

Analogous expressions relate  $G$  to  $g$ .

## B. Bogoliubov transformation

To diagonalize the Hamiltonian, we express the bosonic operators by canonical coordinate and momentum operators  $\Phi_\nu(\mathbf{q}) := \Phi(\mathbf{q} + \mathbf{Q}_\nu)$  and  $\Pi_\nu(\mathbf{q}) := \Pi(\mathbf{q} + \mathbf{Q}_\nu)$  via the relations

$$\Phi_\nu(\mathbf{q}) = \frac{1}{\sqrt{2}} (b_{\mathbf{q} + \mathbf{Q}_\nu} + b_{-\mathbf{q} - \mathbf{Q}_\nu}^\dagger), \quad (11a)$$

$$\Pi_\nu(\mathbf{q}) = \frac{1}{\sqrt{2}i} (b_{-\mathbf{q} - \mathbf{Q}_\nu} - b_{\mathbf{q} + \mathbf{Q}_\nu}^\dagger). \quad (11b)$$

In terms of these operators, the spin-wave Hamiltonian reads

$$\mathcal{H}_{\text{sw}} = \frac{1}{2} \int_{\mathbf{q}, \nu, \nu'} \{ \Pi_\nu^\dagger(\mathbf{q}) \mathbf{M}^{-1}_{\nu, \nu'}(\mathbf{q}) \Pi_{\nu'}(\mathbf{q}) + \Phi_\nu^\dagger(\mathbf{q}) \mathbf{K}_{\nu, \nu'}(\mathbf{q}) \Phi_{\nu'}(\mathbf{q}) \}, \quad (12)$$

with the inverse mass matrix  $\mathbf{M}^{-1} = \mathbf{F} - \mathbf{G}$  and the coupling matrix  $\mathbf{K} = \mathbf{F} + \mathbf{G}$ . As a result of the invariance of the Hamiltonian under the replacement  $\tilde{S}^x(\mathbf{r}) \rightarrow \sigma(\mathbf{r}) \tilde{S}^x(\mathbf{r})$ ,  $\tilde{S}^y(\mathbf{r}) \rightarrow \sigma(\mathbf{r}) \tilde{S}^y(\mathbf{r})$  one can easily derive the symmetry conditions

$$\mathbf{K} = \sigma \mathbf{M}^{-1} \sigma, \quad (13a)$$

$$\mathbf{M}^{-1} = \sigma \mathbf{K} \sigma, \quad (13b)$$

where we have introduced the Hermitian matrix  $\sigma_{\nu, \nu'} := (1/N) \sum_{\mathbf{a}} e^{-i(\mathbf{Q}_\nu - \mathbf{Q}_{\nu'}) \cdot \mathbf{a}} \sigma(\mathbf{a})$ . To simplify notation, we suppress arguments  $\mathbf{q}$  which may be considered as fixed during the diagonalization in  $\nu$  space and use the pseudo-Dirac notation  $|\Phi\rangle\rangle := \sum_{\nu} \Phi_\nu | \nu \rangle\rangle$ ,  $|\Pi\rangle\rangle := \sum_{\nu} \Pi_\nu | \nu \rangle\rangle$  with the Cartesian basis  $| \nu \rangle\rangle$ ,  $\nu = 1, \dots, N$ . After performing the canonical transformation  $|\Phi\rangle\rangle = \mathbf{M}^{-1/2} |\tilde{\Phi}\rangle\rangle$ ,  $|\Pi\rangle\rangle = \mathbf{M}^{1/2} |\tilde{\Pi}\rangle\rangle$  the Hamiltonian can be rewritten as

$$\mathcal{H}_{\text{sw}} = \frac{1}{2} \int_{\mathbf{q}} \{ \langle \langle \tilde{\Pi} | \tilde{\Pi} \rangle \rangle + \langle \langle \tilde{\Phi} | \mathbf{M}^{-1/2} \mathbf{K} \mathbf{M}^{-1/2} | \tilde{\Phi} \rangle \rangle \}, \quad (14)$$

and we still have to diagonalize  $\mathbf{M}^{-1/2} \mathbf{K} \mathbf{M}^{-1/2} = \mathbf{W}^2$  with Hermitian  $\mathbf{W} := \mathbf{M}^{-1/2} \sigma \mathbf{M}^{-1/2}$ . Introducing an orthonormal eigenbasis  $\{ |\alpha\rangle \}, \alpha = 1, \dots, N$  of this matrix,  $\mathbf{W} |\alpha\rangle = \xi_\alpha |\alpha\rangle$ , and defining  $\omega_\alpha := |\xi_\alpha|$ , we can transform to normal coordinates

$$\tilde{\Phi}_\nu = \sum_\alpha \omega_\alpha^{-1/2} \langle \langle \nu | \alpha \rangle \rangle \tilde{\Phi}_\alpha, \quad (15a)$$

$$\tilde{\Pi}_\nu = \sum_\alpha \omega_\alpha^{1/2} \langle \langle \alpha | \nu \rangle \rangle \tilde{\Pi}_\alpha, \quad (15b)$$

and obtain

$$\mathcal{H}_{\text{sw}} = \frac{1}{2} \sum_\alpha \int_{\mathbf{q}} \omega_\alpha \{ \tilde{\Pi}_\alpha^\dagger \tilde{\Pi}_\alpha + \tilde{\Phi}_\alpha^\dagger \tilde{\Phi}_\alpha \}. \quad (16)$$

Transforming back to corresponding bosonic operators  $\tilde{\Phi}_\alpha(\mathbf{q}) = (1/\sqrt{2}) [b_\alpha(\mathbf{q}) + b_\alpha^\dagger(-\mathbf{q})]$ ,  $\tilde{\Pi}_\alpha(\mathbf{q}) = (1/\sqrt{2}i) [b_\alpha(-\mathbf{q}) - b_\alpha^\dagger(\mathbf{q})]$  we obtain the final diagonal bosonic representation of the spin-wave Hamiltonian:

$$\mathcal{H}_{\text{sw}} = \sum_\alpha \int_{\mathbf{q}} \omega_\alpha(\mathbf{q}) \left\{ \frac{1}{2} + b_\alpha^\dagger(\mathbf{q}) b_\alpha(\mathbf{q}) \right\}. \quad (17)$$

Thus, as the result of the above diagonalization we obtain  $\omega_\alpha(\mathbf{q})$  as the magnon dispersion relation with the band index  $\alpha$ .

We would like to remark that the  $|\nu\rangle\rangle$  space contains a common subspace of eigenvectors of the matrices  $\sigma$ ,  $\mathbf{M}^{-1}$ , and  $\mathbf{K}$  with vanishing eigenvalues. This subspace is  $h$  dimensional, where  $h$  is the number of holes in the magnetic unit cell. These zero modes are an artifact of the introduction of spins  $\tilde{\mathbf{S}}$  on the hole sites. Since these spins are decoupled from all other spins, each of them corresponds to a mode with zero energy. All above manipulations, including, e.g., the calculation of  $\mathbf{M}^{1/2}$  and  $\omega_\alpha^{-1}$ , are well defined on the orthogonal subspace of physical spins.

### C. Structure factor

In this section we proceed to calculate the zero-temperature structure factor

$$\mathcal{S}(\mathbf{k}, \omega) := \sum_F \sum_{j=x,y,z} |\langle F | S^j(\mathbf{k}) | 0 \rangle|^2 \delta(\omega - \omega_F). \quad (18)$$

Here,  $|0\rangle$  denotes the ground state (magnon vacuum) characterized by  $b_\alpha(\mathbf{q})|0\rangle = 0$  and we consider only single-magnon states  $|F\rangle$  with excitation energy  $\omega_F := E_F - E_0$ . Since

$$\begin{aligned} \mathcal{S}^z(\mathbf{k}) &= S \sum_{\nu'} \delta(\mathbf{k} - \mathbf{Q}_{\nu'}) \sigma(\mathbf{Q}_{\nu'}) \\ &\quad - \sum_{\nu'} \sigma(\mathbf{Q}_{\nu'}) \int_{\mathbf{k}''} b^\dagger(\mathbf{k}'') b(\mathbf{k} - \mathbf{Q}_{\nu'} + \mathbf{k}'') \end{aligned} \quad (19)$$

with  $\sigma(\mathbf{Q}) := 1/N \sum_{\mathbf{a}} e^{-i\mathbf{Q}\cdot\mathbf{a}} \sigma(\mathbf{a})$  preserves the magnon number, it contributes only to the elastic part of the structure factor,

$$\mathcal{S}^{\text{el}}(\mathbf{k}, \omega) \propto S^2 \sum_{\mathbf{Q}} \delta(\mathbf{k} - \mathbf{Q}) |\sigma(\mathbf{Q})|^2 \delta(\omega). \quad (20)$$

To calculate the inelastic part of the structure factor (which has contributions of order  $S$  only from  $j=x,y$ ) we express these spin components by the bosonic operators using the transformations derived in Sec. III B,

$$\begin{aligned} \mathcal{S}^x(\mathbf{q} + \mathbf{Q}_\nu) &\approx \sqrt{S} \sum_{\nu'} \sigma^{(2)}(\mathbf{Q}_\nu - \mathbf{Q}_{\nu'}) \tilde{\Phi}_{\nu'}(\mathbf{q}) \\ &= \sqrt{\frac{S}{2}} \sum_{\alpha, \nu'} \sigma^{(2)}(\mathbf{Q}_\nu - \mathbf{Q}_{\nu'}) \omega_\alpha^{-1/2} \langle \langle \nu' | \mathbf{M}^{-1/2} | \alpha \rangle \rangle \\ &\quad \times [b_\alpha(\mathbf{q}) + b_\alpha^\dagger(-\mathbf{q})], \end{aligned} \quad (21a)$$

$$\begin{aligned} \mathcal{S}^y(\mathbf{q} + \mathbf{Q}_\nu) &\approx \sqrt{S} \sum_{\nu'} \sigma(\mathbf{Q}_\nu - \mathbf{Q}_{\nu'}) \tilde{\Pi}_{\nu'}^\dagger(\mathbf{q}) \\ &= i \sqrt{\frac{S}{2}} \sum_{\alpha, \nu'} \sigma(\mathbf{Q}_\nu - \mathbf{Q}_{\nu'}) \omega_\alpha^{1/2} \langle \langle \nu' | \mathbf{M}^{1/2} | \alpha \rangle \rangle \\ &\quad \times [b_\alpha(\mathbf{q}) - b_\alpha^\dagger(-\mathbf{q})], \end{aligned} \quad (21b)$$

where we have defined  $\sigma^{(2)}(\mathbf{Q}) := 1/N \sum_{\mathbf{a}} e^{-i\mathbf{Q}\cdot\mathbf{a}} \sigma^2(\mathbf{a})$ . Since the contributing final states are just given by the one-magnon states  $|F\rangle = b_\alpha^\dagger(\mathbf{q})|0\rangle$ , it is easy to calculate the inelastic part of the structure factor. Using the relations  $\sigma^2 \mathbf{M}^{-1/2} |\alpha\rangle\rangle = \sigma \mathbf{M}^{1/2} \mathbf{W} |\alpha\rangle\rangle = \xi_\alpha \sigma \mathbf{M}^{1/2} |\alpha\rangle\rangle$  and  $\sigma^2 \mathbf{M}^{-1/2} |\alpha\rangle\rangle = \mathbf{M}^{-1/2} |\alpha\rangle\rangle$ , we obtain

$$\mathcal{S}^{\text{in}}(\mathbf{q} + \mathbf{Q}_\nu, \omega) = S \sum_\alpha S_\alpha(\mathbf{q} + \mathbf{Q}_\nu) \delta(\omega - \omega_\alpha(\mathbf{q})), \quad (22a)$$

$$S_\alpha(\mathbf{q} + \mathbf{Q}_\nu) = \langle \langle \nu | \mathbf{M}^{-1/2} | \alpha \rangle \rangle \frac{1}{\omega_\alpha} \langle \langle \alpha | \mathbf{M}^{-1/2} | \nu \rangle \rangle. \quad (22b)$$

At this point it may be helpful to remind that  $\mathbf{q}$  is an implicit argument of  $\omega_\alpha$ ,  $\mathbf{M}^{-1/2}$ , and  $|\alpha\rangle\rangle$ . The periodicity  $\omega_\alpha(\mathbf{q}) = \omega_\alpha(\mathbf{q} + \mathbf{Q})$  of the eigenfrequencies is absent in the structure factor since the coupling of an external field to a spin-wave wave vector  $\mathbf{k} = \mathbf{q} + \mathbf{Q}$  depends on  $\mathbf{Q}$ .

## IV. RESULTS

We now evaluate the above general analytic expressions for the magnon dispersion and the structure factor. Thereby we focus on our minimalistic model (cf. Sec. II) with stripe spacings  $p=3, 4$ , and  $5$ , since these values correspond to doping concentrations in various experimental works as mentioned in the Introduction. The explicit comparison to experiments is postponed to Sec. V.

For later reference, we briefly recall that for the undoped two-dimensional antiferromagnet (which is recovered by

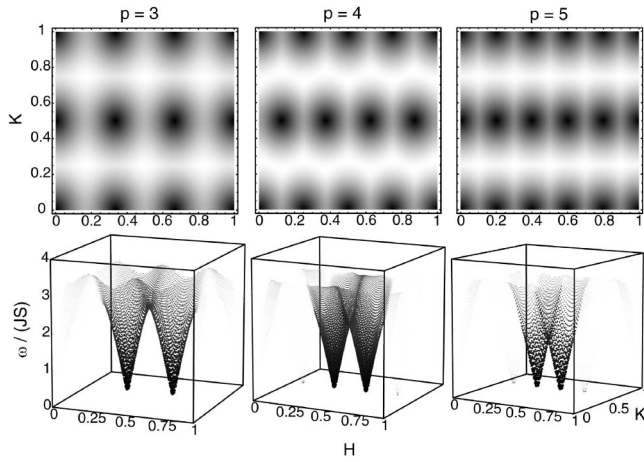


FIG. 2. Acoustical band for vertical stripes with spacings  $p = 3, 4, 5$  and  $\lambda = 0.5$ . The upper row shows density plots of the spin-wave dispersion, where dark regions correspond to low-energy values. The lower row shows the acoustical band in the  $(H, K, \omega)$  space including the weight of the inelastic structure factor, where larger weight corresponds to darker points with larger size.

our model in the limit  $p \rightarrow \infty$ , the spin-wave dispersion is given by

$$\omega_{\text{AF}}(\mathbf{k}) = 2JS \sqrt{4 - [\cos(2\pi H) + \cos(2\pi K)]^2}. \quad (23)$$

[From now on, we refer to wave vectors  $\mathbf{k} = (H, K)$  in units of  $2\pi/a$ .] It vanishes at the antiferromagnetic wave vector  $\mathbf{k}_{\text{AF}} = (\frac{1}{2}, \frac{1}{2})$ , where the structure factor shows maximal intensity. To leading order in  $\delta\mathbf{q} = \mathbf{k} - \mathbf{k}_{\text{AF}}$ , the low-energy spin-wave excitations are characterized by an isotropic dispersion  $\omega_{\text{AF}} \approx v_{\text{AF}} |\delta\mathbf{q}|$  with a spin-wave velocity  $v_{\text{AF}} = \sqrt{8}JSa$ .

### A. Vertical case

For vertical stripes a possible magnetic unit cell is given by the basis vectors  $\mathbf{A}^{(1)} = (0, 2)$  and  $\mathbf{A}^{(2)} = (p, 0)$  for odd or  $\mathbf{A}^{(2)} = (p, 1)$  for even  $p$ . Therefore we have  $N = 2p$  lattice sites per unit cell (cf. Fig. 1) and  $2p$  eigenvalues  $\omega_a(\mathbf{q})$ . Two of them (corresponding to the number of holes) vanish identically and we obtain  $p - 1$  twofold degenerate physical bands. This degeneracy results from the equivalence of the two sublattices.

The lowest, acoustical band has zeros at the magnetic superstructure lattice vectors. Within the Brillouin zone of the square lattice (we choose  $0 \leq H, K < 1$ ), the vectors  $\mathbf{Q}_v$  are located at  $(j/p, 0)$  and  $(j/p, 1/2)$  for odd  $p$  or  $((j/p) + (1/2p), 1/2)$  for even  $p$  (with  $0 \leq j < p$ ). In the upper row of Fig. 2, we show  $\omega(\mathbf{k})$  for the acoustical band as a density plot, where black corresponds to  $\omega = 0$  and white to the upper band edge.

Although the dispersion relation obeys the symmetry  $\omega(\mathbf{k}) = \omega(\mathbf{k} + \mathbf{Q})$  corresponding to the period of the magnetic unit cell, this symmetry is absent in the structure factor. In the lower row of Fig. 2, the acoustic band is replotted in the  $(H, K, \omega)$  space using darker and thicker dots for points with larger values of the structure factor (22). In agreement with experiments, the weights are concentrated near the lowest

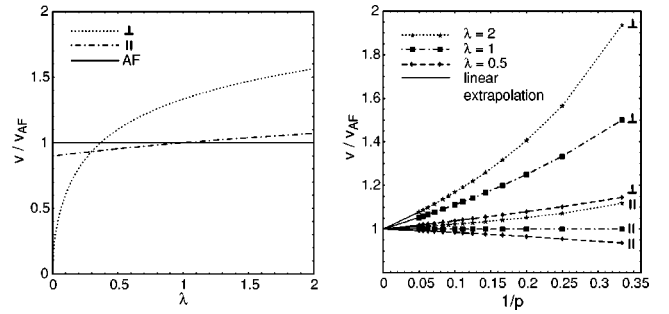


FIG. 3. Spin-wave velocities  $v_{\perp}$  and  $v_{\parallel}$  for vertical stripes with spacing  $p = 4$  as a function of  $\lambda$  (left panel) and as a function of  $1/p$  for different couplings  $\lambda$  (right panel; lines are a guide to the eye).

harmonic incommensurate wave vectors  $\mathbf{Q} = ((1/2) \pm (1/2p), 1/2)$ . Higher harmonics of the superstructure are much weaker as already noticed in Ref. 5.

To study the anisotropy of the dispersion next to the satellite positions, we calculate the spin-wave velocities  $v_{\perp}$  and  $v_{\parallel}$  perpendicular and parallel to the stripe orientation (cf. Fig. 3). For  $\lambda = 0$ , where the coupling between the domains is switched off,  $v_{\perp}$  is zero and  $v_{\parallel}$  remains finite. With increasing  $\lambda$  both velocities increase,  $v_{\perp}$  more strongly than  $v_{\parallel}$ . There exists a value  $\lambda^*$  with isotropic velocities,  $v_{\perp} = v_{\parallel}$ . For  $p = 4$  we find  $\lambda^* \approx 0.3$ . In the limit  $p \rightarrow \infty$  both velocities converge to  $v_{\text{AF}}$  as expected, for  $p \gg 1$  we find  $v_{\perp, \parallel} / v_{\text{AF}} - 1 \propto 1/p$ . In the special case  $\lambda = 1$ , the velocities are given by

$$v_{\parallel} = v_{\text{AF}}, \quad (24a)$$

$$v_{\perp} = \frac{p}{p-1} v_{\text{AF}} \quad (24b)$$

for purely geometric reasons. In this case, all spins are interacting in terms of the topology and strength of the exchange couplings exactly like in the antiferromagnet. The only difference lies in the insertion of strings of holes, which effectively stretch the lattice and increase the velocity by a factor  $p/(p-1)$  in the perpendicular direction.

We now focus on the line  $\mathbf{k} = (H, \frac{1}{2})$  containing the satellites, along which we plot all  $p - 1$  magnon bands in Fig. 4 for a variety of  $p$  and  $\lambda$ . For  $\lambda < 1$  and  $\lambda > 1$  the bands are separated by gaps. (In this context, “gaps” are not necessarily real gaps showing up in the density of states, they are apparent gaps along the chosen line.) Only for  $\lambda = 1$ , the structure seems to consist of displaced and intersecting antiferromagnetic bands. The value  $\lambda = 1$  is special for the reasons explained above, which also imply that the bandwidth must coincide with the antiferromagnet. The purely geometric effect entails just a more complicated band structure.

To the extent to which our stripe model provides a valid description of the magnetic excitations in the materials where the  $\pi$  resonance was observed, the resonance frequency has to be identified with  $\omega(\mathbf{k}_{\text{AF}})$  from the lowest magnon band, provided  $\omega(\mathbf{k}_{\text{AF}}) > 0$  and the structure factor has significant weight. From Fig. 4 one recognizes that for  $\lambda < 1$  this is always the acoustical band. On the other hand,

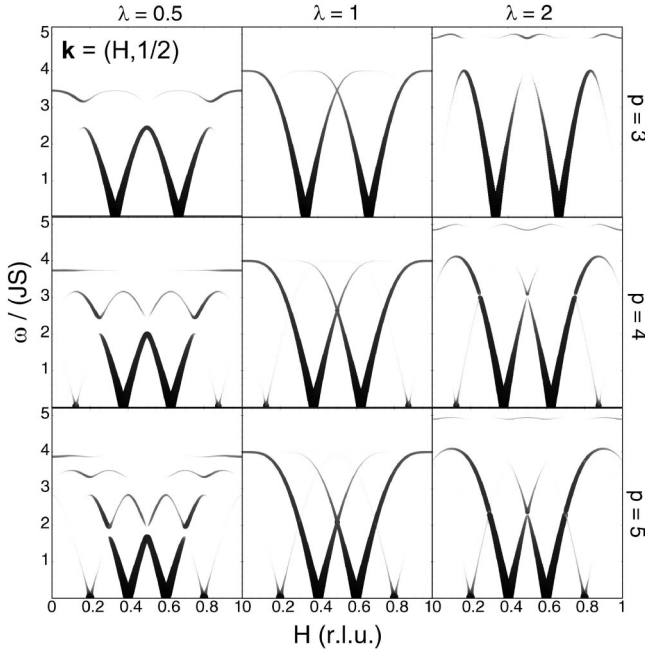


FIG. 4. Band structure for vertical stripes along the  $(H, 0.5)$  direction with different spacings  $p$  and couplings  $\lambda$ . Darker and larger points correspond to a larger weight of the inelastic structure factor.

for  $\lambda > 1$  higher bands may yield a stronger resonance (see case  $p = 3$  and  $\lambda = 2$ ). In Fig. 5, we illustrate the dependence of  $\omega_\pi$  on  $\lambda$  and  $p$ .

For  $p$  large enough such that  $v_{\parallel} \approx v_{AF}$  and the magnon dispersion is roughly linear between the main satellite and  $\mathbf{k}_{AF}$ , we may estimate

$$\omega_\pi \approx v_{AF} \frac{\pi}{pa}. \quad (25)$$

This estimate becomes exact for small  $1/p$  and represents the linear asymptotics in Fig. 5 (right). Deviations grow with decreasing  $p$  and increasing deviation of  $\lambda$  from 1.

### B. Diagonal case

For diagonal stripes there are more subtle differences between even and odd stripe spacings  $p$ . Since the basis vectors

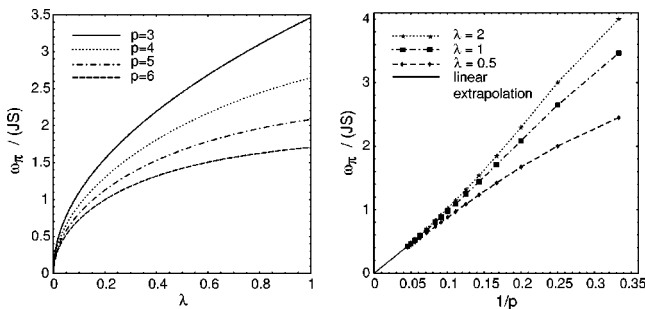


FIG. 5. The resonance frequency  $\omega_\pi$  for vertical stripes as a function of  $\lambda$  for different spacings  $p$  (left) and as a function of  $1/p$  for different couplings  $\lambda$  (right; lines are a guide to the eye).

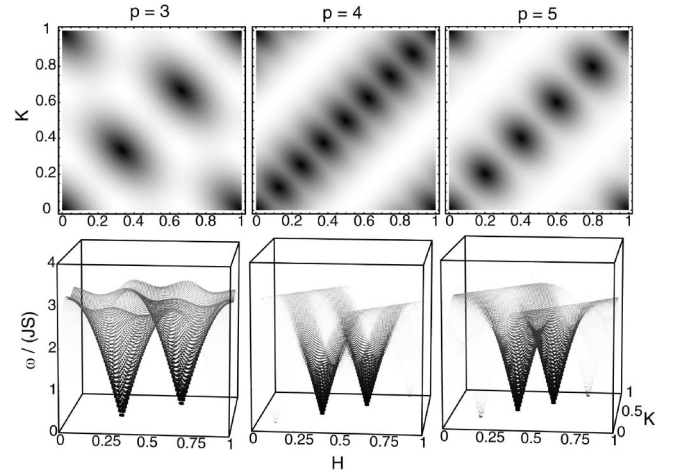


FIG. 6. Acoustical band for diagonal stripes with spacings  $p = 3, 4, 5$  for  $\lambda = 1$  plotted in analogy to Fig. 2.

of the magnetic unit cell can be chosen as  $\mathbf{A}^{(1)} = (-1, 1)$  and  $\mathbf{A}^{(2)} = (p, 0)$  for odd or  $\mathbf{A}^{(2)} = (2p, 0)$  for even  $p$  (cf. Fig. 1), we have one hole and  $p - 1$  spins per unit cell for odd  $p$  and twice the number of holes and spins for even  $p$ . Like in the vertical case, the number of eigenvalues vanishing identically corresponds to the number of holes, the number of bands is given by half of the number of spins per unit cell, and the bands are twofold degenerate.

All magnetic Bragg peaks are located along the line  $\mathbf{Q} = (H, H)$  with  $H = j/p$  for odd and  $H = j/(2p)$  for even  $p$  (cf. Fig. 6). In the case  $p = 3$  we can calculate the dispersion analytically and find

$$\omega(\mathbf{k}) = 2JS \{ \sin^2[\pi(H - K)] + \lambda \sin^2[\pi(2H + K)] + \lambda \sin^2[\pi(H + 2K)] \}^{1/2}. \quad (26)$$

Along the  $\mathbf{k} = (H, H)$  direction this relation simplifies to

$$\omega(H, H) = \sqrt{2\lambda} JS |\sin(3\pi H)|. \quad (27)$$

Though the case  $p = 3$  with a single band is the simplest possible, we find several critical points in the dispersion, which should result in a nontrivial shape of the density of states  $\rho(\omega) \sim \int_{\mathbf{k}} \delta(\omega - \omega(\mathbf{k}))$ . Therefore we calculate this quantity just to illustrate that even for this simplest case,  $\rho(\omega)$  shows interesting features strongly depending on the effective coupling  $\lambda$ . The numerically calculated density of states is plotted in Fig. 7 for different values of  $\lambda$ . The van Hove singularities are located at the energies of the critical points in the dispersion. The dependence of these energies on the coupling  $\lambda$  is also shown in this figure. Due to a finite numerical resolution the van Hove singularities are not resolved if they are too close to each other and their precise shape is not reproduced, e.g., at the energies of the saddle points,  $\rho(\omega)$  should diverge logarithmically.

Calculating the weight by the structure factor of the bands we find the strongest intensity near the zeros of the acoustic band at the satellite positions

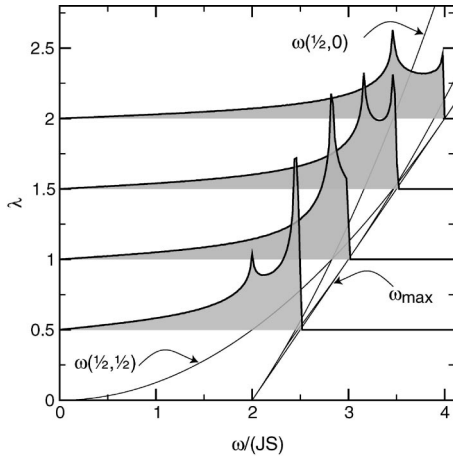


FIG. 7. Density of states  $\rho(\omega)$  (height of shaded area in arbitrary units) for diagonal stripes with spacing  $p=3$  and different couplings  $\lambda$ . The thin lines correspond to the energies of the critical points in the dispersion. There are up to four inequivalent ones, at  $\mathbf{k}=(\frac{1}{2},\frac{1}{2})$ ,  $\mathbf{k}=(\frac{1}{2},0)$ , the upper band edge with  $\omega_{\max}$  and a possible additional critical point.

$$\mathbf{Q} = \left( \frac{1}{2} \pm \frac{1}{2p}, \frac{1}{2} \pm \frac{1}{2p} \right)$$

for all  $p$ . The behavior of the spin-wave velocities  $v_{\perp}$  and  $v_{\parallel}$  (cf. Fig. 8) is similar to the vertical case.

Along the  $\mathbf{k}=(H,H)$  direction, the acoustical band is separated by finite gaps from the optical bands for  $\lambda \neq 2$ . For  $\lambda=2$ , the band structure again seems to consist of intersecting displaced antiferromagnetic bands. In contrast to the vertical case, the special value of  $\lambda$  is now 2 since for this value the sum of the exchange couplings to neighboring spins is as large as in the antiferromagnet. However, for diagonal stripes the topology of the couplings is different from the antiferromagnet.

For odd  $p$ , the  $\pi$  resonance results from the excitation of acoustical magnons since the lowest band has a finite  $\omega(\mathbf{k}_{\text{AF}})$  with a relatively strong weight. In contrast, for even  $p$  the frequency and the weight of the acoustical band vanish at  $\mathbf{k}_{\text{AF}}$ . In this case, the  $\pi$  resonance should therefore be ascribed to optical magnons. For  $\lambda=2$ , the  $\pi$  resonance results from the common edge of the acoustical and optical bands (cf. Fig. 9). With increasing coupling  $\lambda$ , the resonance energy

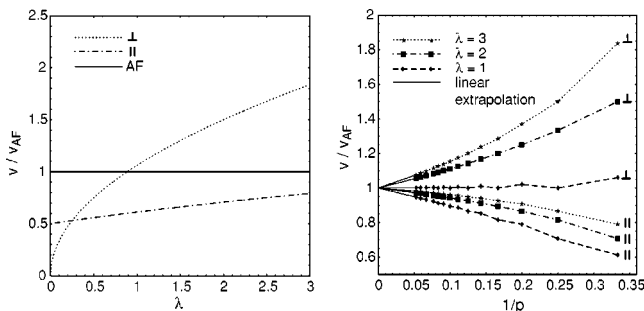


FIG. 8. Spin-wave velocities  $v_{\perp}$  and  $v_{\parallel}$  for diagonal stripes with spacing  $p=3$  as a function of  $\lambda$  (left) and as a function of  $1/p$  for different couplings  $\lambda$  (right; lines are a guide to the eye).

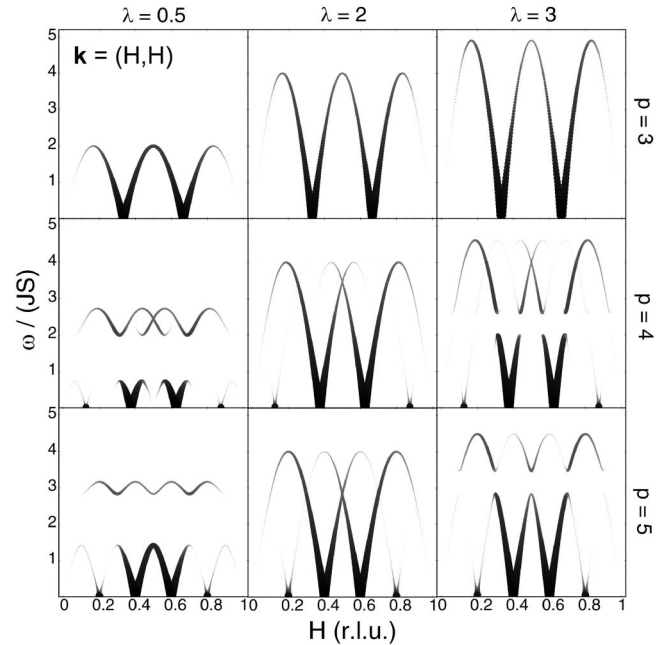


FIG. 9. Band structure for diagonal stripes along the  $(H,H)$  direction with different spacings  $p$  and couplings  $\lambda$ .

increases. In contrast to vertical stripes, the resonance energy remains finite in the limit  $\lambda \rightarrow 0$  for even  $p$  where it arises from an optical band. (cf. Fig. 10). Like for the vertical case,  $\omega_{\pi}$  decreases with increasing stripe spacing, for  $p \gg 1$  according to  $\omega_{\pi} \propto 1/p$ . Since resonance comes from different bands for even and odd  $p$  the  $\pi$ ,  $\omega_{\pi}$  is a nonmonotonous function of  $p$ . For this reason,  $\omega_{\pi}(p)$  is plotted in Fig. 10 separately for the two cases.

## V. DISCUSSION

We now discuss our findings in comparison to experimental data on the spin dynamics, which are obtained predominantly from neutron scattering. As a result of this comparison we wish to advocate that the simple stripe model provides a fair account of the spin dynamics at not too low energies. At very low energies, spin gaps may occur, e.g., due to spin anisotropies [as in nonsuperconducting LNO (Ref. 24) and

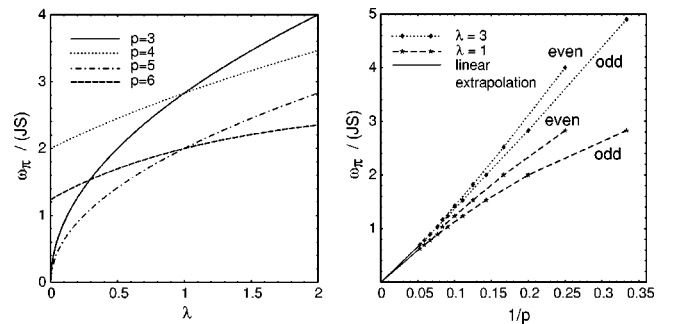


FIG. 10. Resonance frequency  $\omega_{\pi}$  for diagonal stripes as a function of  $\lambda$  for different spacings  $p$  (left) and as a function of  $1/p$  for different couplings  $\lambda$  (right; lines are a guide to the eye distinguishing even and odd  $p$ ).

TABLE I. Basic parameters of the undoped parent compounds: number of layers in the crystalline unit cell, spin, nearest-neighbor spin spacing, nearest-neighbor antiferromagnetic exchange coupling, and spin-wave velocity. NA stands for not available.

Material	No. of layers	$S$	$a(\text{Å})$	$J(\text{meV})$	$v_{\text{AF}}(\text{eV Å})$	References
LNO	1	1	3.8	30	0.32	20,34,24
LCO	1	$\frac{1}{2}$	3.8	135	0.85	26,27
YBCO	2	$\frac{1}{2}$	3.9	125	NA	20
BSCCO	2	$\frac{1}{2}$	3.8	140	NA	20

LCO (Ref. 25)], due to the coupling of spins to the superconducting order parameter (as in superconducting cuprates, see below), or simply due to the absence of antiferromagnetic order (for too small  $\lambda$ ). Our model could straightforwardly be generalized to account for the first origin. The inclusion of superconductivity would require a major extension.

In Table I, we have collected basic parameters for various undoped compounds setting the fundamental physical scales. In Table II spin dynamics data for specific stripe structures are compiled.

### A. LSNO

We start the comparison with LSNO which displays diagonal stripes and where integer values of  $p$  are particularly stable<sup>31,32</sup> due to a lock-in of the stripes into the atomic structure. In this material, static stripes (i.e., stripes that are visible down to  $\omega=0$ ) are seen at wave vectors  $\mathbf{Q}_v$ .<sup>33</sup> For  $p=3$ , the spin dynamics at higher energies has been measured in detail.<sup>16</sup> Similar data are also available for noninteger  $p$ , e.g.,  $p=3.75$ .<sup>10</sup>

Experiments<sup>24,34</sup> on *undoped* material are in agreement with two-dimensional (2D) spin-wave theory for the antiferromagnet with  $J\approx 30$  meV. This exchange coupling corresponds to an isotropic spin-wave velocity<sup>24</sup>  $v_{\text{AF}}=\sqrt{8SJ}a=0.32$  eV Å since  $S=1$  and  $a\approx 3.8$  Å. This agreement is

TABLE II. Spin dynamics data for different materials at various doping levels characterized by the critical temperature  $T_c$ , stripe period  $p$  and orientation (diagonal/vertical), resonance frequency  $\omega_\pi$ , and gap frequency  $\omega_{\text{gap}}$ . NA stands for not available.

Material	$T_c(\text{K})$	$p$	$\omega_\pi$ (meV)	$\omega_{\text{gap}}$ (meV)	References
LSNO	0	3( $d$ )	80	$\leq 28$	16
LSCO	$\approx 38$	4( $v$ )	NA	3.5	37,38,17
LSCO	10	6( $v$ )	25	$\leq 1.1$	38
LSCO	0	$\approx 43(d)$	7	0	48
YBCO	90	5( $v$ )	41	28	39,28,14
YBCO	63	NA	35	28	29
YBCO	59	NA	26	16	39
YBCO	39	8( $v$ )	23	10	18
BSCCO	91	NA	43	NA	30,43
BSCCO	83	NA	38	NA	43

reasonably good over a wide energy range  $\omega\gtrsim 30$  meV up to the band edge at  $\omega\approx 125$  meV, at low energies  $\omega\lesssim 15$  meV deviations (gaps) appear<sup>24</sup> due to a uniaxial spin anisotropy and weak interlayer couplings.

The spin dynamics of the stripe system was examined for  $p=3.75$  due to oxygen doping<sup>10</sup> as well as for  $p=3$  with Sr doping.<sup>16</sup> In the first case, a reduced velocity  $v_{\parallel}\approx 0.6v_{\text{AF}}$  was found in direction parallel to the stripes,  $v_{\perp}$  was not resolved. In the second case, the velocity was measured in both directions and found to be remarkably isotropic and close to the value of the undoped system:  $v_{\parallel}\approx 0.30$  eV Å and  $v_{\perp}\approx 0.35$  eV Å. The overall shape of the magnon dispersion was sinusoidal with an upper edge at  $\omega_\pi\approx 80$  meV.

In our theory, this sinusoidal shape for  $p=3$  is well reproduced [compare Fig. 9 and Eq. (27)]. The ratio  $\omega_\pi/(JS)\approx 2.7$  is consistent with  $\lambda\approx 0.9$ . For this value of  $\lambda$ ,  $v_{\perp}\approx v_{\text{AF}}$  and  $v_{\parallel}\approx 0.67v_{\text{AF}}$ . Although we find  $v_{\parallel}$  to be smaller than in Ref. 16, the overall agreement is very satisfying and provides strong support for our case that the spin dynamics can be well understood from a stripe model. Small quantitative deviations may be attributed to the simplicity of our model using only two types of exchange couplings.

Remarkably,  $\lambda\approx 0.9$  implies that the spin exchange across a stripe is *not much smaller* than within an antiferromagnetic domain. It is important to keep in mind that  $\lambda$  *must not* be too small to preserve magnetic order. A quantum Monte Carlo analysis<sup>35</sup> of coupled two-leg ladders ( $S=1$ ) indicates a quantum phase transition into a disordered state at  $\lambda\approx 0.011$ . Below this value, stripe order would be destroyed by quantum fluctuations.

Within our approach we can estimate also the two-magnon signal accessible by Raman spectroscopy. We may compare our single-magnon density  $\rho(\omega)$  to the two-magnon scattering intensity at frequency  $2\omega$ . Certainly, this can be made only on a qualitative level, since  $\rho$  was calculated neglecting weight factors (which would change the shape of spectra but not the frequency of resonances) and because linear spin-wave theory does not include interactions between magnons. Nevertheless, it is instructive to compare the outcome from our model for the diagonal case  $p=3$  with an experiment by Blumberg *et al.*<sup>36</sup> on LSNO. In this experiment, two magnetic resonances are observed at  $\omega\approx 4.6J$  and  $\omega\approx 3J$ . For  $\lambda\approx 0.9$  we expect a singularity in the single-magnon density at  $\omega\approx 2.7JS$  (see Fig. 7), which would correspond to a two-magnon resonance at  $\omega\approx 5.4JS$ . If corrections due to magnon interactions are modest, the resonance of the theory could be identified with the upper experimental one. Then the resonance at the lower frequency cannot be understood. On the other hand, for  $\lambda$  not too close to 1 the single-band structure for  $p=3$  would lead to several well-separated extrema but contradict the above determination of  $\lambda$ . In particular, for  $\lambda<1$ , the additional resonance lies above  $\omega_\pi$  since it arises from extrema close to the upper band edge and there is only a saddle point at  $\mathbf{k}_{\text{AF}}$ . This apparent contradiction might be resolved if either interaction corrections are large, additional exchange interaction are important, or the lower experimental resonance is of different origin.

## B. Cuprates

In the present study, we *assume* the presence of charge stripes and evaluate the spin dynamics for a simple model. The question of why stripes are formed and how stripe formation is related to superconductivity therefore cannot be addressed. In particular, the simple spin-only model misses the coupling of spin fluctuations to the superconducting order parameter. Consequently, our analysis misses the opening of a spin gap due to superconductivity. Therefore, the spin dynamics for  $\omega < \omega_{\text{gap}}$  is masked by superconductivity (see Table II). Nevertheless, one can expect the stripelike spin dynamics to remain visible in superconducting samples for  $\omega > \omega_{\text{gap}}$ .

Such a gap has been observed in experiments on LSCO [e.g.,  $\omega_{\text{gap}} \approx 3.5$  meV near optimal doping with  $T_c = 38.5$  K;<sup>17,37,38</sup> a gap smaller than 1.1 meV for underdoped samples with  $T_c = 12$  K and  $T_c = 25$  K (Ref. 38)] and on YBCO (e.g.,  $\omega_{\text{gap}} \approx 10$  meV for a highly underdoped material with  $T_c = 39$  K;<sup>18</sup>  $\omega_{\text{gap}} \approx 16$  meV for a moderately underdoped material with  $T_c = 59$  K;<sup>39</sup>  $\omega_{\text{gap}} \approx 30$  meV for near optimal doping with<sup>14</sup>  $T_c = 89$  K). For YBCO there is evidence<sup>40</sup> for a proportionality between  $\omega_{\text{gap}} \approx 3.8T_c$  which is not far away from the BCS weak-coupling limit with  $\omega_{\text{gap}} = 3.52T_c$ .

Furthermore—and more importantly in the present context—there is evidence for such a (rough) proportionality not only between  $T_c$  and  $\omega_{\text{gap}}$  but also between  $T_c$  and  $\omega_\pi$  ( $\omega_\pi \approx 5T_c$  for underdoped YBCO,<sup>41,42</sup>  $\omega_\pi \approx 5.4T_c$  for underdoped and overdoped<sup>43</sup> BSCCO). From our theory, we expect  $\omega_\pi$  to be roughly inversely proportional to  $p$ , see Eq. (24) and Fig. 10. At low doping,  $p$  should be inversely proportional to the doping level ( $x + 2\delta$ ), i.e.,  $\omega_\pi$  should be proportional to the doping level. Such a relation was found in a previous theoretical study of the Hubbard model,<sup>44</sup> where it was attributed to a particle-particle collective mode. Although our approach is technically much less involved, it provides an alternative explanation which is not in contradiction with the previous one, since stripe order itself can be considered as a collective phenomenon that can be derived from the Hubbard model<sup>1,2</sup> (for collective magnetic excitations in a Hubbard model with stripes, see also Refs. 45 and 46).

On the other hand, at larger doping there is no simple relation between the doping level and  $p$ . In YBCO, for example, the charge-transfer mechanism between the  $\text{CuO}_2$  plane and the CuO chains interferes. In LSCO it is well documented that  $p$  saturates at  $p = 4$  for  $x \geq 0.12$ .<sup>47</sup> Beyond that point (which corresponds to optimum doping<sup>47</sup>), additional holes may populate the antiferromagnetic domains without affecting their period  $p$ . However, these excess holes may suppress the antiferromagnetic exchange coupling in analogy to holes in the spin-glass phase (Ref. 10 reports the corresponding suppression of the spin-wave velocity). Hence, the effective  $J$  and, consequently, also  $\omega_\pi$  may shrink with overdoping as seen in experiments on BSCCO.<sup>43</sup>

For LSCO, so far no direct evidence for a  $\pi$  resonance has been found. This could be simply because the resonance intensity is expected to be only  $\sim 10\%$  of the total magnetic

scattering.<sup>12</sup> However, if the  $\pi$  resonance—in the sense of a merger of the incommensurations—can be attributed to magnons in stripes which are particularly well established for LSCO, one definitely should expect such a resonance. For underdoped LSCO ( $p = 6$ ,  $T_c = 25$  K) there is evidence for  $\omega_\pi = 25$  meV (where satellites merge at the antiferromagnetic wave vector).<sup>38</sup> A similar signal was observed at even lower doping in the spin-glass phase ( $\omega_\pi = 7$  meV for  $p \approx 43$ ).<sup>48</sup>

Like for LSNO, we may use the values of  $J$ ,  $p$ , and  $\omega_\pi$  to estimate  $\lambda$  for the cuprates. For YBCO with  $J = 125$  meV,  $p = 5$ , and  $\omega_\pi = 41$  meV,<sup>14,40</sup> we obtain  $\lambda \sim 0.07$  from the left panel of Fig. 5. If we take  $J = 135$  meV and  $\omega_\pi = 25$  meV for LSCO with  $p = 6$ ,<sup>38</sup> an even smaller value  $\lambda \sim 0.04$  is found.

From this result we may predict where the resonance  $\omega_\pi$  should be expected in LSCO near optimal doping ( $p = 4$ ). For  $J = 135$  meV and  $\lambda = 0.04 - 0.07$  we find  $\omega_\pi \approx 40 - 52$  meV. While the resulting values for  $\omega_\pi$  have a certain spread, they suggest that the resonance frequency should be at least as large as in optimally doped YBCO.

In the experiments known to us, the considered energy range was simply too small to detect the resonance for optimally doped LSCO:  $\omega \leq 6$  meV in Ref. 37,  $\omega \leq 10$  meV in Refs. 47 and 49,  $\omega \leq 16$  meV in Ref. 17. However, from pulsed neutron scattering, evidence has been found for a broad peak in the momentum-integrated susceptibility between<sup>50,51</sup> 40 and 70 meV, which could be ascribed to the  $\pi$  resonance.

Apparently,  $\lambda$  seems to be significantly smaller in the cuprates than in the nickelates. At the same time,  $S$  is smaller (although  $J$  is larger). Therefore, one may wonder whether static magnetic stripe order is already destroyed by quantum fluctuations without invoking competing orders leading to a gap. For  $S = \frac{1}{2}$  the coupling needs to satisfy  $\lambda \geq 0.3$  to stabilize spin order for  $p = 3$ ,<sup>22,35</sup> while for  $p = 4$  a finite  $\lambda > 0$  is sufficient.<sup>22</sup> For  $p = 5$  (as for every odd  $p$ ) one again expects a finite critical  $\lambda$ . If the interstripe coupling is below this value, the presence of a spin gap can be understood also within the spin-only model.

## C. Conclusion

In summary, we find that the spin fluctuations of stripes can provide a simple and valuable description of the dynamics observed in high- $T_c$  compounds and related materials. Already our minimalistic spin-only model provides an accurate account of experiments on LSNO and possibly also a unifying framework for incommensurate response and the  $\pi$  resonance in the cuprates. While such a framework has been suggested recently,<sup>15</sup> it is analyzed and evaluated here for the most transparent case of integer periods  $p$ . Our results unravel the evolution of the band structure with  $p$  for diagonal and vertical stripe configurations. Likewise, we have explicitly determined the dependence of characteristic spin-wave velocities and of the resonance frequency on  $p$  and  $\lambda$ . Thereby, we postulate that the  $\pi$  resonance reflects the magnon frequency  $\omega_\pi$  of the lowest-lying band with nonvanish-

ing weight. In particular,  $\omega_\pi$  was found to be roughly inversely proportional to  $p$  in agreement with experiments.

Hopefully, future experiments can provide more direct evidence for the  $\pi$  resonance also in LSCO. This would also relax the controversial question, whether spin excitations in LSCO and YBCO are analogous<sup>7</sup> or not.<sup>14</sup> If stripe magnons indeed explain the spin dynamics at intermediate energies, as we expect, they would provide a unifying framework for understanding the spin dynamics above the gap scale. Then the stripe physics would be also of great importance as base-ment for superconductivity as low-energy phenomenon.

Naturally, several aspects remain unexplained by our minimalistic theory. For example, our model cannot be expected to explain why the magnetic incommensuration disappears at  $T_c$  in YBCO (Ref. 14) while charge order is visible up to 300 K.<sup>18</sup> Probably this is a question to the stripe-forming mechanism and to a possible coupling between the order parameters for stripe order and superconductivity. In

LSCO, the vicinity of soft phonons and structural instabilities may help to stabilize stripes at temperatures above the superconducting transition.

For future studies it would be interesting to include effects of the bilayer coupling present in YBCO and BSCCO, of the weak 3D coupling present in all materials, as well as spin anisotropy, more complicated spin interactions (e.g., four-spin cyclic exchange<sup>20,21</sup>), excitations beyond spin waves (e.g., double-spin excitations<sup>36</sup>), mobility of spins, and effects of disorder, to name just a few.

## ACKNOWLEDGMENTS

We gratefully acknowledge helpful discussions with M. Braden, M. Grüninger, B. Keimer, E. Müller-Hartmann, T. Nattermann, and G. S. Uhrig. This project was supported financially by Deutsche Forschungsgemeinschaft (SFB608).

- 
- <sup>1</sup>J. Zaanen and O. Gunnarsson, Phys. Rev. B **40**, 7391 (1989).  
<sup>2</sup>H.J. Schulz, J. Phys. (Paris) **50**, 2833 (1989).  
<sup>3</sup>K. Machida, Physica C **158**, 192 (1989).  
<sup>4</sup>J.M. Tranquada, D.J. Buttrey, V. Sachan, and J.E. Lorenzo, Phys. Rev. Lett. **73**, 1003 (1994).  
<sup>5</sup>J.M. Tranquada, B.J. Sternlieb, J.D. Axe, Y. Nakamura, and S. Uchida, Nature (London) **375**, 561 (1995).  
<sup>6</sup>P. Dai, H.A. Mook, and F. Dogan, Phys. Rev. Lett. **80**, 1738 (1998).  
<sup>7</sup>H.A. Mook, P. Dai, S.M. Hayden, G. Aeppli, T.G. Perring, and F. Dogan, Nature (London) **395**, 580 (1998).  
<sup>8</sup>C. Howald, H. Eisaki, N. Kaneko, and A. Kapitulnik, cond-mat/0201546 (unpublished).  
<sup>9</sup>J.E. Hoffman, E.W. Hudson, K.M. Lang, V. Madhavan, E. Eisaki, S. Uchida, and J.C. Davis, Science **295**, 466 (2002).  
<sup>10</sup>J.M. Tranquada, J.D. Axe, N. Ichikawa, A.R. Moodenbaugh, Y. Nakamura, and S. Uchida, Phys. Rev. Lett. **78**, 338 (1997).  
<sup>11</sup>B. Khaykovich, Y.S. Lee, R.W. Erwin, S. Lee, S. Wakimoto, K.J. Thomas, M.A. Kastner, and R.J. Birgeneau, cond-mat/0112505 (unpublished).  
<sup>12</sup>P. Bourges, in *The Gap Symmetry and Fluctuations in High-Temperature Superconductors*, edited by J. Bok, G. Deutscher, D. Pavuna, and S. A. Wolf (Plenum Press, New York, 1998).  
<sup>13</sup>H. He, P. Bourges, Y. Sidis, C. Ulrich, L.P. Regnault, S. Pailhes, N.S. Berzigiarova, N.N. Kolesnikov, and B. Keimer, Science **205**, 1045 (2002).  
<sup>14</sup>P. Bourges, Y. Sidis, H.F. Fong, L.P. Regnault, J. Bossy, A. Ivanov, and B. Keimer, Science **288**, 1234 (2000).  
<sup>15</sup>C.D. Batista, G. Ortiz, and A.V. Balatsky, Phys. Rev. B **64**, 172508 (2001).  
<sup>16</sup>P. Bourges, Y. Sidis, M. Braden, K. Nakajima, and J. Tranquada, cond-mat/0203187 (unpublished).  
<sup>17</sup>B. Lake, G. Aeppli, T.E. Mason, A. Schröder, F.D. McMorro, K. Lefmann, M. Isshild, M. Nohara, H. Takagi, and S.M. Hayden, Nature (London) **400**, 43 (2000).  
<sup>18</sup>H.A. Mook, P. Dai, and F. Dogan, Phys. Rev. Lett. **88**, 097004 (2002).  
<sup>19</sup>We follow the common practice where modes are called “commensurate” at the antiferromagnetic wave vector and “incommensurate” at the satellite positions irrespective of the value of  $p=d/a$ .  
<sup>20</sup>S. Sugai, M. Sato, T. Kobayashi, J. Akimitsu, T. Ito, H. Takagi, S. Uchida, S. Hosoya, T. Kajitani, and T. Fukuda, Phys. Rev. B **42**, 1045 (1990).  
<sup>21</sup>E. Müller-Hartmann and A. Reischl, Eur. Phys. J. B **28**, 173 (2002).  
<sup>22</sup>J. Tworzydło, O.Y. Osman, C.N.A. van Duin, and J. Zaanen, Phys. Rev. B **59**, 115 (1999).  
<sup>23</sup>E. Manousakis, Rev. Mod. Phys. **63**, 1 (1991).  
<sup>24</sup>K. Nakajima, K. Yamada, S. Hosoya, T. Omata, and Y. Endoh, J. Phys. Soc. Jpn. **62**, 4438 (1993).  
<sup>25</sup>B. Keimer, R.J. Birgeneau, A. Cassanho, Y. Endoh, M. Greven, M.A. Kastner, and G. Shirane, Z. Phys. B: Condens. Matter **91**, 373 (1993).  
<sup>26</sup>K.B. Lyons, P.A. Fleury, J.P. Remeika, A.S. Cooper, and T.J. Negran, Phys. Rev. B **37**, 2353 (1988).  
<sup>27</sup>S.M. Hayden, G. Aeppli, H.A. Mook, S.-W. Cheong, and Z. Fisk, Phys. Rev. B **42**, 10 220 (1990).  
<sup>28</sup>H.A. Mook, M. Yethiraj, G. Aeppli, T.E. Mason, and T. Armstrong, Phys. Rev. Lett. **70**, 3490 (1993).  
<sup>29</sup>P. Dai, M. Yethiraj, H.A. Mook, T.B. Lindemer, and F. Dogan, Phys. Rev. Lett. **77**, 5425 (1996).  
<sup>30</sup>H.F. Fong, P. Bourges, Y. Sidis, L.P. Regnault, A. Ivanov, G.D. Guk, N. Koshizuka, and B. Keimer, Nature (London) **398**, 588 (1999).  
<sup>31</sup>C.H. Chen, S.-W. Cheong, and A.S. Cooper, Phys. Rev. Lett. **71**, 2461 (1993).  
<sup>32</sup>S.-W. Cheong, H.Y. Hwang, C.H. Chen, B. Batlogg, L.W. Rupp, Jr., and S.A. Carter, Phys. Rev. B **49**, 7088 (1994).  
<sup>33</sup>S.M. Hayden, G.H. Lander, J. Zarestky, P.J. Brown, C. Stassis, P. Metcalf, and J.M. Honig, Phys. Rev. Lett. **68**, 1061 (1992).  
<sup>34</sup>K. Yamada, M. Arai, Y. Endoh, S. Hosoya, K. Nakajima, T. Perring, and A. Taylor, J. Phys. Soc. Jpn. **60**, 1197 (1991).

- <sup>35</sup>M. Matsumoto, C. Yasuda, S. Todo, and H. Takayama, *Phys. Rev. B* **65**, 014407 (2001).
- <sup>36</sup>G. Blumberg, M.V. Klein, and S.-W. Cheong, *Phys. Rev. Lett.* **80**, 564 (1998).
- <sup>37</sup>K. Yamada, S. Wakimoto, G. Shirane, C.H. Lee, M.A. Kastner, S. Hosoya, M. Greven, Y. Endoh, and R.J. Birgeneau, *Phys. Rev. Lett.* **75**, 1626 (1995).
- <sup>38</sup>S. Petit, A.H. Moudden, B. Hennion, A. Vietkin, and A. Revcolevschi, *Physica B* **234-236**, 800 (1997).
- <sup>39</sup>J. Rossat-Mignod, L.P. Regnault, C. Vettier, P. Bourges, P. Bulet, J. Bossy, J.Y. Henry, and G. Lapertot, *Physica C* **185-189**, 86 (1991).
- <sup>40</sup>P. Dai, H.A. Mook, R.D. Hunt, and F. Dogan, *Phys. Rev. B* **63**, 054525 (1999).
- <sup>41</sup>H.F. Fong, B. Keimer, D.L. Milius, and I.A. Aksay, *Phys. Rev. Lett.* **78**, 713 (1997).
- <sup>42</sup>P. Dai, H.A. Mook, S.M. Hayden, G. Aeppli, T.G. Perring, R.D. Hunt, and F. Dogan, *Science* **284**, 1344 (1999).
- <sup>43</sup>H. He, Y. Sidis, P. Bourges, G.D. Gu, A. Ivanov, N. Koshizuka, B. Liang, C.T. Lin, L.P. Regnault, E. Schoenher, and B. Keimer, *Phys. Rev. Lett.* **86**, 1610 (2001).
- <sup>44</sup>E. Demler and S.-C. Zhang, *Phys. Rev. Lett.* **75**, 4126 (1995).
- <sup>45</sup>M. Ichioka, E. Kaneshita, and K. Machida, *J. Phys. Soc. Jpn.* **70**, 818 (2001).
- <sup>46</sup>E. Kaneshita, M. Ichioka, and K. Machida, *J. Phys. Soc. Jpn.* **70**, 866 (2001).
- <sup>47</sup>K. Yamada, C.H. Lee, K. Kurahashi, J. Wada, S. Wakimoto, S. Ueki, Y. Endoh, S. Hosoya, G. Shirane, R.J. Birgeneau, M. Greven, M.A. Kastner, and Y.J. Kim, *Phys. Rev. B* **57**, 6165 (1998).
- <sup>48</sup>M. Matsuda, M. Fujita, K. Yamada, R.J. Birgeneau, M.A. Kastner, H. Hiraka, Y. Endoh, S. Wakimoto, and G. Shirane, *Phys. Rev. B* **62**, 9148 (2000).
- <sup>49</sup>C.-H. Lee, K. Yamada, Y. Endoh, G. Shirane, R.J. Birgeneau, M.A. Kastner, M. Greven, and Y.-J. Kim, *J. Phys. Soc. Jpn.* **69**, 1170 (2000).
- <sup>50</sup>K. Yamada, Y. Endoh, C.H. Lee, S. Wakimoto, M. Arai, K. Ubukata, M. Fujita, S. Hosoya, and S.M. Bennington, *J. Phys. Soc. Jpn.* **64**, 2742 (1995).
- <sup>51</sup>M. Arai, T. Arakawa, M. Fujita, S. Wakimoto, K. Yamada, Y. Endoh, G. Aeppli, T.E. Mason, and S.M. Hayden, *Czech. J. Phys. (Suppl.)* **46**, 1147 (1996).